

Experimental verification of quantized conductance for microwave frequencies in photonic crystal waveguides

W. Dai,¹ B. Wang,¹ Th. Koschny,^{1,2} and C. M. Soukoulis^{1,2}

¹Ames Laboratory-USDOE, and Department of Physics and Astronomy, Iowa State University, Ames, Iowa 50011, USA

²Institute of Electronic Structure and Lasers (IESL), FORTH, and Department of Material Science and Technology, University of Crete, 71110 Heraklion, Crete, Greece

(Received 8 July 2008; published 28 August 2008)

We report experiments that demonstrate the quantization of the conductance of photonic crystal waveguides. To obtain a diffusive wave, we have added all the transmitted channels for all the incident angles. The conductance steps have equal height and a width of one half the wavelength used. Detailed numerical results agree very well with the novel experimental results.

DOI: [10.1103/PhysRevB.78.073109](https://doi.org/10.1103/PhysRevB.78.073109)

PACS number(s): 42.70.Qs, 41.20.-q, 71.20.-b

Quantization of different physical quantities is one of the interesting phenomena in science. The quantization occurs because of the wave nature of particles. One quantity that gives strong quantization is the electrical conductance g , the inverse of the resistance. It is very difficult to calculate the transport properties of small devices analytically. Landauer was the first one to make the connection between the conductance and the transmission coefficient.¹ He showed that $G = (e^2/\hbar\pi)T/(1-T)$, where T is the transmission coefficient. If one has a perfect metal $T=1$, then $G \rightarrow \infty$ and therefore $R \rightarrow 0$, as expected for a perfect metal. In 1981, Soukoulis and Economou² proved, by using the Kubo-Greenwood formula, that for one-dimensional (1D) systems $G = (e^2/\hbar\pi)T$. There was a fierce controversy in 1980s regarding which formula was correct,³ since the Economou-Soukoulis formula gives a finite value for the resistance for the perfect metal. The experiments^{4,5} resolved this issue and indeed it was found that $G = (e^2/\hbar\pi)T$. Extensions to higher dimension^{6,7} were achieved for G and it was shown that for a multichannel wire the dimensionless conductance g

$$g = G \left/ \left(\frac{e^2}{\hbar\pi} \right) \right. = \sum_{n,m=1}^{N_c} |t_{nm}|^2, \quad (1)$$

where t_{nm} is the transmission coefficient between incident mode n and output mode m . The same set of modes N_c are used for the incident and output modes. For classical waves the total T is equivalent to the dimensionless conductance⁸ in electronic systems $T=g$. For the ideal waveguide configuration, g gives the number of propagation modes inside the waveguide.

The key idea of Landauer was to relate the resistance of the sample with its transmission. So the idea of quantization of conductance can be also obeyed by all types of waves, electromagnetic waves, acoustic, and elastic waves. It is amazing that the only experiment⁹ that has been done with waves is the transmission of a slit of variable width for a given wavelength of $\lambda = 1.55 \mu\text{m}$. Similar to its electronic counterpart, the optical conductance of a structure is described as the total light transmitted through the structure from a diffusive illumination (an isotropic incoherent incident wave). So the conductance g for classical waves is dimensionless. In the experiment of Montie *et al.*⁹ a two-

dimensional (2D) diffuser was used to achieve the diffusive illumination. The diffuser was essentially a 2D random array of scatterers through which the normally incident plane wave scatters diffusively and isotropically. The diffused light passed through a metal slit and the transmitted light was collected. The result showed that the optical conductance increases in a staircase fashion. A new step occurs when the slit width $W = n\lambda/2$ ($n=1, 2, 3, \dots$) i.e., a new mode is enabled in the slit.

Photonic crystals (PCs) can be designed to have a band gap that prohibits wave propagation in a certain frequency range.¹⁰ Line defects of PCs can confine light with frequencies within the band gap inside the channel and act as waveguides. PC waveguides have been studied extensively and many applications have been proposed.¹⁰ However, the concept of optical conductance was not applied to PC waveguides until recently^{11,12} and no experimental work has been reported to our knowledge. In this Brief Report we study the optical conductance of photonic crystal waveguides, both numerically and experimentally. We will demonstrate experimentally that the optical conductance of a 2D PC waveguide in microwaves has the similar staircase effect as the metal slit.

We design the working frequency of the waveguide at microwave region, which makes the PC easy to be fabricated. One of the main experimental difficulties is the need of diffusive waves. It is easy to be achieved at optical wavelengths by a diffuser. For microwaves, a large enough random array of scatterers are needed to act as a diffuser. Since the wavelength is now of the order of centimeter, the diffuser must be really big in size and the intensity of the transmitted waves will be too weak to be used efficiently. So we apply Eq. (1) in experiments for classical waves. We measure the transmitted power for each incident plane wave with different incident angle separately and sum them up to obtain the conductance of electromagnetic waves.¹¹

The PC we study is a 2D square array of square alumina rods. The lattice constant is $a = 11 \text{ mm}$ and the square rods are of dimension $d = 3.18 \text{ mm}$ with relative permittivity $\epsilon = 9.8$ and height $h = 15 \text{ cm}$. It has a band gap between 9.43 and 12.78 GHz for TM modes (electric field parallel to the rods). The waveguide is formed by two closely separated pieces of PC slabs with a size of $25a \times 4a$ each. The width of

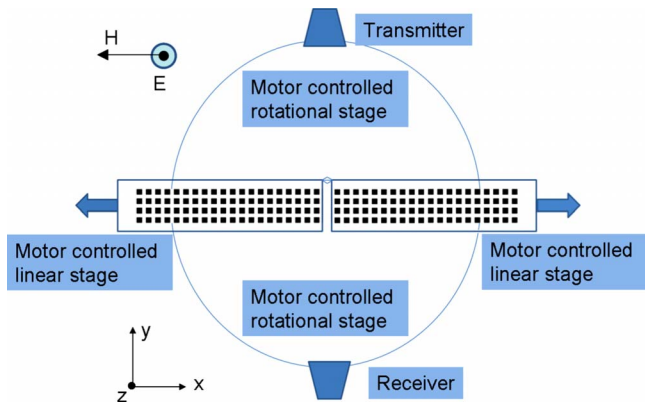


FIG. 1. (Color online) An illustration of the experimental setup.

the waveguide (W) can be varied by changing the distance between the two PC slabs. HP8510B network analyzer and a pair of horn antennas are used to measure the transmission. The antennas are mounted on motorized rotational stages which can move along a circle with a radius of 30 cm and centering at the middle of the entrance of the waveguide. So both the incident and outgoing angle can be controlled. (See Fig. 1 for details).

The experimental result of the optical conductance of the PC waveguide is shown together with numerical simulations in Fig. 2. We see that the optical conductance increases in a staircase manner with the increase of the waveguide width. The steps forming the staircases have essentially the same height and a new step appears at each integer multiple of $\lambda/2$. Notice that the first conductance step does not start at $W/\lambda=0.5$. This is because that for the photonic crystal channel the boundaries are not well defined and the field decays exponentially inside the photonic crystal. So the waveguide is wider than W .

We use the commercial software COMSOL Multiphysics to do the numerical simulations. The simulation results of three frequencies are shown in Fig. 3. To understand the shape of optical conductance curves, the band structure of the PC with the channel are calculated using the supercell technique. When the channel width increases, some bands move downward into the band gap of the PC. Figure 4 shows the band structure when $W=38.673$ mm. There are four impurity bands inside the band gap. The experimental fre-

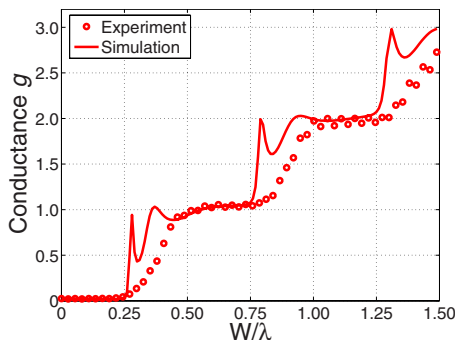


FIG. 2. (Color online) The experimental and numerical results of optical conductance of a PC waveguide at 10 GHz.

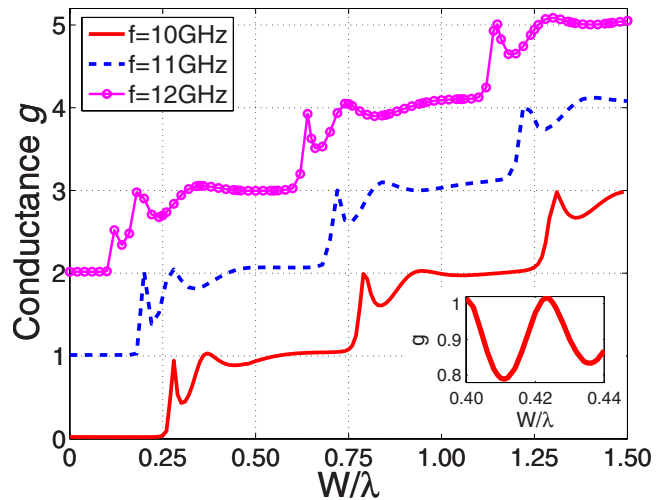


FIG. 3. (Color online) The numerical results of optical conductance. The working frequencies are 10, 11, and 12 GHz. The curves of 11 and 12 GHz are shifted vertically. The PC has 4 layers along the channel direction. Inset: g vs W/λ when $f=10$ GHz and the PC has 40 layers.

quency $f=10$ GHz crosses the three impurity bands. It means the channel can support three propagation modes. The propagation wave vectors k_{\parallel} of the modes can be read from the horizontal axis. Figure 5 shows the relations between the propagation wave vectors of the propagation modes and the width of the channel when $f=10$ GHz based on the band-structure simulations. The figure demonstrates clearly that the first propagation mode appears when $W/\lambda=0.25$ and one more propagation mode when the width increase $\lambda/2$. Comparing with Fig. 3, it is clear that the optical conductance steps describes the number of propagation modes supported by the channel.

The oscillation of the optical conductance curves can also be explained by the propagation wave vectors of the channel modes. A natural explanation about the conductance oscillations is the Fabry-Pérot interference, the interference between the multiple reflection of waves inside the waveguide. The phase difference between two succeeding reflection equals the propagation phase $2k_{\parallel}L$ (L is the length of the

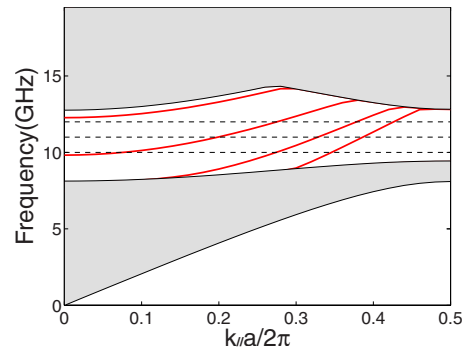


FIG. 4. (Color online) Band structure of PC with the channel. The channel width is $W=38.673$ mm. The dark area is the band area of a perfect PC. The dash lines shows three working frequencies. The red solid curves shows the impurity bands in the band gap of a perfect PC.

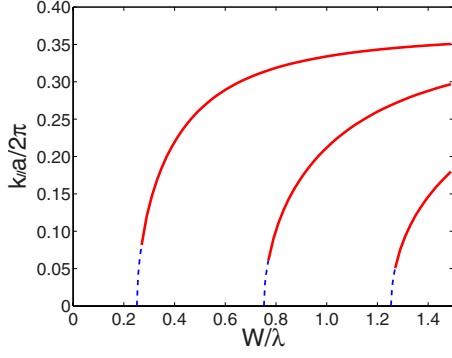


FIG. 5. (Color online) Wave vectors of the propagation modes vs the width of the channel. The solid lines are gotten from band structure of PC with the channel. The dash lines are extrapolation of the solid lines.

channel) plus the phase change of the reflections at the entrance and the exit of the channel. The reflection ratio changes with the channel width. To prove that the conductance oscillations are due to the Fabry-Pérot interference, we calculated the optical conductance curves for a long channel ($L=40a$, $f=10$ GHz). The inset of Fig. 3 shows the simulation result. When the channel width changes from 0.41λ to 0.43λ , the oscillation has a full period. The reflection ratio is a continuous function of the channel width. So the reflection ratio will not change too much during the period since the width does not change too much. Then we neglect them and compare the propagation phases only. When $W/\lambda=0.411$, 0.423 , 0.436 , the conductance curve has a dip, a peak, and another dip. The propagation phases are $2k_{||}L=36.10\pi$, 37.09π , 38.09π , respectively. The phase differences between a dip and its neighboring peak are 0.99π and 1.00π . They agree with the Fabry-Pérot explanation.

From Fig. 2 we can see that the onset of the staircases in experiments and simulations are in good agreement. However, the Fabry-Pérot oscillations are missing in the experiments. The major reason is that, while in simulations the model is perfectly 2D, we do not have an ideal 2D system in experiments. The source we get from a radiating horn antenna is a confined beam. When it encounters the PC structure, while the main part is propagating in xy plane, the beam also scatters out of the plane. Since the receiving antenna only collects the transmitted power in the xy plane where it sits, not all the transmitted power is obtained. At the onset of the staircase, more power is lost due to the multiple reflection. So the experimental curve is lower than the one obtained by simulations and the Fabry-Pérot resonances are missing.

We also studied the optical conductance of a perfect electric conductor (PEC) channel, which serves as a simplified model of the photonic crystal waveguides. Analytical calculations starting from Maxwell's equations¹³ are performed to understand the mechanism behind the stairs.

Suppose $y=0$ is the interface of the air and the PEC channel. The half-space $y<0$ is the air and $y>0$ is the PEC channel. $x=0$ is the middle of the PEC channel (see the inset of Fig. 7).

In TM mode, the incident wave is

$$E_z^{\text{inc}} = \exp[i(k_{||}y + k_{\perp}x)]. \quad (2)$$

Here $k_{||}=k_0 \cos \theta$; $k_{\perp}=k_0 \sin \theta$. k_0 is the wave vector in air; θ is the incident angle. The reflected wave is the composition of plane waves. The total electric field in the air area is

$$E_z^{\text{air}} = \exp[i(k_{||}y + k_{\perp}x)] + \int_{-\infty}^{\infty} dk \rho(k) \exp[i(kx - k_y y)], \quad (3)$$

where $k_y = \sqrt{k_0^2 - k^2}$, and $\rho(k)$ are unknown coefficients.

The channel is infinite long; so the field in the channel is the composition of all the channel modes moving toward $+y$ direction.

$$E_z^{\text{channel}} = \sum_{m=1}^{\infty} A_m \phi_m(x) \exp[i\beta_m y]. \quad (4)$$

Here $\phi_m(x) = \sin[m\pi(x+W/2)/W]$ is the channel mode profile and $\beta_m = \sqrt{k_0^2 - (m\pi/W)^2}$.

We have defined the fields before the channel [Eq. (3)] and in the channel [Eq. (4)] separately. E_z and H_x should be continuous along the interface $y=0$. By using these boundary conditions we can obtain the following set of equations for the unknowns A_n :

$$A_n \gamma_n \beta_n + \sum_{m=1}^{\infty} A_m g_{mn} = I_n. \quad (5)$$

Here

$$I_n = \int_{-W/2}^{W/2} 2k_{||} \exp[ik_{\perp}x] \phi_n(x) dx. \quad (6)$$

$$\gamma_n = \int_{-W/2}^{W/2} \phi_n(x) \phi_n(x) dx = W/2. \quad (7)$$

$$g_{mn} = \frac{1}{2\pi} \int_{-\infty}^{\infty} dk \int_{-W/2}^{W/2} dx \int_{-W/2}^{W/2} dx' \{ \sqrt{k_0^2 - k^2} \times \phi_m(x') \phi_n(x) \exp[ik(x-x')] \}. \quad (8)$$

This method can be applied to TE mode too. Because of space constraints, we would not repeat it here.

The coefficients of the channel models A_n are solved by Eq. (5). Then the optical conductance of the infinite-long channel can be calculated.

We also used COMSOL Multiphysics to simulate the infinite-long channel numerically by inserting a perfect matched layer (PML) (Ref. 14) in the channel. The incoming channel modes are absorbed by PML without reflection. Figure 6 shows the analytic calculation and numerical simulation results. The Fabry-Pérot oscillations disappear since the channel is infinite long. The PEC channel has at least one TE propagation mode no matter how narrow the channel is. So the first step of TE mode begins at $W/\lambda=0$. It is an interesting question why the conductance curves, shown in Fig. 6, of TE and TM modes have different behavior.

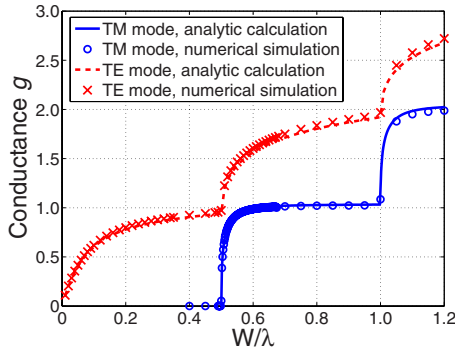


FIG. 6. (Color online) Optical conductance of a infinite-long PEC channel. The first 10 channel modes are chosen in the analytic calculation; COMSOL Multiphysics is used to do the numerical simulations.

Experimental measurements have also been performed and the results are shown together with the simulation results in Fig. 7 for TM case. The experimental curve is smooth and lower than the simulation results, similar with the PC curves.

We can simplify Eq. (5) furthermore. When $k_0W \gg 1$ and $n \ll k_0W$,

$$g_{mn} \approx \begin{cases} \gamma_n \beta_n & \text{if } m = n; \\ 0 & \text{if } m \neq n. \end{cases} \quad (9)$$

So $A_n \approx I_n / 2 \gamma_n \beta_n$.

It means when the channel is wide, we can get the coefficients of the first several modes directly. Then it is easy to

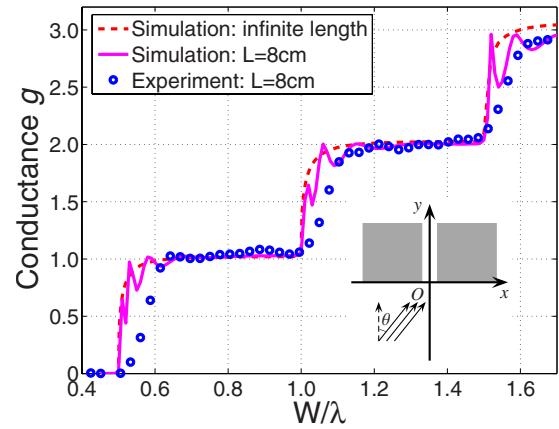


FIG. 7. (Color online) The experimental and numerical results of optical conductance of a PEC channel for TM case. Inset: Diagram of the PEC channel.

prove that the contribution to the optical conductance by one mode converges to 1 when the channel width goes to infinity. This is the reason for the step profile.

We have shown for the first time that the conductance of the photonic crystal waveguide is quantized in microwave frequencies. Quantization does not only occur in small length scales and in the quantum regime but also in long length scales and in the classical regime. We have also introduced new ways to obtain diffusive waves in the microwave region.

This work was partially supported by Ames Laboratory (Contract No. DE-AC0207CH11385) and EU projects Metamorphose and Phoremot.

¹R. Landauer, IBM J. Res. Dev. **1**, 223 (1957); Phys. Lett. **85A**, 91 (1981).

²E. N. Economou and C. M. Soukoulis, Phys. Rev. Lett. **46**, 618 (1981).

³For a historical account of the controversy from two different perspectives, see R. Landauer, IBM J. Res. Dev. **32**, 306 (1988); A. D. Stone and A. Szafer, *ibid.* **32**, 384 (1988).

⁴G. Timp, A. M. Chang, P. Mankiewich, R. Behringer, J. E. Cunningham, T. Y. Chang, and R. E. Howard, Phys. Rev. Lett. **59**, 732 (1987).

⁵B. J. van Wees, H. van Houten, C. W. J. Beenakker, J. G. Williamson, L. P. Kouwenhoven, D. van der Marel, and C. T. Foxon, Phys. Rev. Lett. **60**, 848 (1988); B. J. van Wees, L. P. Kouwenhoven, E. M. M. Willems, C. J. P. M. Harmans, J. E. Mooij, H. van Houten, C. W. J. Beenakker, J. G. Williamson, and C. T. Foxon, Phys. Rev. B **43**, 12431 (1991).

⁶D. S. Fisher and P. A. Lee, Phys. Rev. B **23**, 6851 (1981).

⁷M. Büttiker, Y. Imry, R. Landauer, and S. Pinhas, Phys. Rev. B **31**, 6207 (1985).

⁸M. Stoytchev and A. Z. Genack, Phys. Rev. Lett. **79**, 309 (1997).

⁹E. A. Montie, E. C. Cosman, G. W. 't Hooft, M. B. Van der Mark, and C. W. J. Beenakker, Nature (London) **350**, 594 (1991).

¹⁰See, for example, *Photonic Crystals and Light Localization in the 21st Century*, edited by C. M. Soukoulis (Kluwer, Dordrecht, 2001).

¹¹S. Albaladejo, J. J. Sáenz, M. Lester, L. S. Froufe-Pérez, and A. García-Martín, Appl. Phys. Lett. **91**, 061107 (2007).

¹²L. C. Botten, A. A. Asatryan, N. A. Nicorovici, R. C. McPhedran, and C. M. de Sterke, Physica B (Amsterdam) **394**, 320 (2007).

¹³L. Martín-Moreno, F. J. García-Vidal, H. J. Lezec, A. Degiron, and T. W. Ebbesen, Phys. Rev. Lett. **90**, 167401 (2003); F. J. García-Vidal, H. J. Lezec, T. W. Ebbesen, and L. Martín-Moreno, *ibid.* **90**, 213901 (2003); J. Bravo-Abad, L. Martín-Moreno, and F. J. García-Vidal, Phys. Rev. E **69**, 026601 (2004).

¹⁴*Computational Electrodynamics: The Finite-Difference Time-Domain Method*, edited by A. Taflov and S. C. Hagness (Artech House, Boston, 2000).